ROYAL SOCIETY
OF CHEMISTRY

PAPER

Check for updates

A Janus adhesive hydrogel sheet for preventing postoperative tissue adhesion of intestinal injuries

Jingmei Li,[a] Jiadi Liang,[b] Shanshan Chen,[a] Wucheng Guo,[a] Ting Chen*[a] and Xiqiang Liu [ID] *[a]

Although adhesive hydrogels represent an alternative to surgical sutures for non-invasive tissue wound sealing, those with indiscriminate adhesion fail to hold wounds while inhibiting postoperative tissue adhesion, thus limiting their application in intestinal repair. In this study, an asymmetric adhesive hydrogel sheet composed mainly of polyacrylic acid (PAA) and gelatin (GA) that can be wet-adhered to the surface of intestinal tissue was developed. One side of the GA-PAA hydrogel sheet was complexed with polyvinyl alcohol (PVA), which shielded the excess adhesion based on a physical barrier. Both sides of the PVA/GA-PAA hydrogel showed distinct adhesive and antiadhesive properties. Intriguingly, the anti-adhesive side showed significant anti-adhesion toward specific proteins. The results of animal experiments showed that the PVA/GA-PAA hydrogel could firmly adhere to the intestine to stop leakage and prevent post-operative tissue adhesion two weeks after surgery. The hematoxylin and eosin (H&E) staining results showed that the damaged intestinal serosa was repaired without tissue adhesion. It is believed that the controllable adhesion of the adhesive hydrogel offers better prospects for intestinal repair.

Introduction

Surgical sutures have served as the universal method for wound closure in the clinic; however, stitching suffers from some adverse disadvantages, including being time-consuming and difficult to operate, as well as causing secondary tissue damage.[1–3] More recently, tissue adhesives have attracted increasing attention as alternatives to sutures owing to advantages such as time savings, simple operation, and noninvasivity in terms of tissue damage, avoiding suture-related complications.[4–8] While there are numerous emerging bioadhesive hydrogels, most of them are double-sided adhesives without different adhesion on different surfaces, suffering from unfavorable postoperative tissue adhesion caused by excessive tissue adhesion during the operation process, thus limiting their clinical application in intestinal repair.[9–13]

Postoperative tissue adhesion between intestinal tissue and other organs can lead to a series of complications, such as long-term pelvic pain, intestinal obstruction, and even infertility, and commonly requires a second surgery to relieve the adverse tissue adhesion.[12–14] Current biomaterials such as Interceed, Seprafilm and anti-adhesion liquids can prevent postoperative tissue adhesion; however, they cannot hold tissue due to a lack of tissue adhesion.[14,15] Therefore, it is of clinical significance to

develop biomaterials that can adhere to tissue and concurrently prevent postoperative tissue adhesion. In past studies, adhesive groups on the surface of the adhesive biomaterials were removed by immersion in a non-adhesive ionic solution, which can reduce postoperative tissue adhesion.[16] However, it was demonstrated that a systemic inflammatory reaction was initiated, with the adhesion of specific proteins leading to postoperative tissue adhesion due to the lack of anti-fouling properties.[13] Therefore, biological anti-fouling ability should be taken into consideration for ideal biomaterials for intestine repair in addition to the removal of excessive tissue adhesion.[17] Li *et al.* tried to prepare a polycaprolactone (PCL) film modified by zwitterions to obtain strong biological anti-fouling ability due to the super-hydrophilic surface.[18] It has been reported in some studies that super-hydrophilic zwitterions can contribute to a thin hydration layer on the surface of the modified film, forming a structure similar to the lipid bilayer, blocking the adhesion of cells and proteins, evading recognition by the immune system and inhibiting the inflammatory response.

In addition, it was found that dense hydrophilic structures benefit anti-fouling properties.[16] Wu *et al.* prepared a hydrogel sheet based on PVA with a dense microstructure on the top surface, and its stitching in the abdomen significantly reduced postoperative abdominal adhesion.[19] Lee *et al.* prepared a dense film using PVA and gelatin, which effectively reduced postoperative abdominal adhesion.[20] Shi *et al.* developed a dense physical barrier film based on carboxymethyl cellulose, which effectively inhibited postoperative abdominal adhesion.[21] Therefore, modifying the surface of adhesive biomaterials with

[a]*Department of Stomatology, Nanfang Hospital, Southern Medical University, Guangzhou 510515, P.R. China. E-mail: 547698545@qq.com; haoyunljm@163.com*
[b]*Center of Stomatology, Shunde Hospital of Southern Medical University, Foshan 528000, P.R. China*

dense hydrophilic physical barriers will help to achieve ideal intestinal repair.[22]

In order to meet this challenge, we prepared an adhesive GA-PAA hydrogel sheet based on a UV-curing process. The hydrogen bonding force generated by the abundant carboxyl groups on the surface of the hydrogel contributes to rapid tissue adhesion. The covering PVA membrane shields the excessive adhesion of carboxyl groups on the top surface. The hydrogen bonding and mechanical interlocking between PVA and GA-PAA generate a dense surface, thus forming a composite hydrogel sheet with an asymmetric porous surface and tissue adhesion, which can contribute to intestine repair without postoperative tissue adhesion.

Experimental section

Materials

All chemical reagents were purchased from Sigma-Aldrich and utilized without further purification unless otherwise mentioned. To obtain the hydrogel sheet, acrylic acid (AA), gelatin methacrylate (gelMA, from porcine skin with 80% substitution), gelatin (GA, from porcine skin) and Irgacure 2959 were utilized for the preparation of the adhesive substance. PVA (with 99% hydrolyzed, Mw 115 000) was used for the anti-adhesive substance. To better remove the adhesive hydrogel from the mold, we customized a mold using Teflon materials with an as-prepared groove with a thickness of 210 μm.

Preparation of PVA/GA-PAA hydrogel sheet

The PVA/GA-PAA hydrogel sheet was mainly prepared using a two-step process. In brief, the adhesive GA-PAA hydrogel was prepared using a prepolymer solution including 30% (w/w) AA, 0.1% (w/w) gelMA, 10% (w/w) GA and 0.1% (w/w) Irgacure 2959 by UV-curing for 20 min in a mold. Next, 5% (w/w) PVA solution was uniformly coated on the surface of GA-PAA after drying for 10 minutes in the oven (50 °C). Lastly, the PVA/GA-PAA hydrogel was completely dried to form a sheet, taken out of the mold and stored at −20 °C. The PVA/GA-PAA hydrogel sheet was used in the as-made state. To prepare the GA-PAA hydrogel sheet as the control group, the process was same as for the PVA/GA-PAA hydrogel sheet but without PVA coating.

Chemical structure

Fourier transform infrared (FTIR) spectra of the GA-PAA and PVA/GA-PAA hydrogel sheets samples were measured to confirm the expected chemical structure. Samples for FTIR measurements were ground with 1 wt% KBr and pressed into pellets, and absorption peaks were measured in the spectral range of 4000 to 400 cm^{-1} using an FTIR spectrometer (Avatar 360, USA). High-resolution X-ray photoelectron spectroscopy (XPS) of C and N was conducted using the Escalab Xi+ instrument (ThermoFisher, U.S.). The detection conditions were 23.5 eV pass energy utilizing Ar$^+$ gun neutralization to compensate.

SEM observation

The PVA/GA-PAA hydrogel sheets after lyophilization were fixed on a copper platform, sprayed with gold for 180 s, and observed utilizing a Quanta 250 FEG field SEM (Thermo Fisher, Talos F200x, USA), operating at an accelerating voltage of 20 kV. For a better comparison of the two-sided morphology of the hydrogel sheet samples, the samples were obtained under the same conditions and the top surface and bottom surface were from the same sample.

Adhesion test

To measure the adhesive performance of PVA/GA-PAA hydrogel sheets, one side of the intestinal tissue was fixed on stiff backings using cyanoacrylate glue. The adhesive side of the PVA/GA-PAA hydrogel sheet sample was adhered to the fresh intestinal surface under persistent pressing for 5 seconds with a 1 kPa force. The samples were then subjected to a lap-shear test according to the standard conditions of ASTM F2256 at a stable rate of 20 mm min^{-1} utilizing a mechanical testing machine (10 N load-cell, Instron 5967, USA). The intact stress–strain curves were recorded until the hydrogel sheet sample broke away from the tissue.

Mechanical test

The hydrogel sheets in the as-made and water-equilibrated state were trimmed into a dog-bone shape for the stress–strain experiment ($L = 30$ mm, $W = 10$ mm). The Young modulus of the hydrogel sheet sample was measured using a tension test at a stable rate of 30 mm min^{-1} utilizing a mechanical testing machine (10 N load-cell, Instron 5967, USA). To better observe the stretching effect, the tensile length of the samples was photographed using a digital camera before breakage.

Protein resistance property

The hydrogel sheet samples were submerged and incubated in 2 mg mL^{-1} fibrin solution and bovine serum albumin (BSA) for 2 hours at 37 °C, respectively. The sheet samples were gently taken out of the solution, washed at least four times using deionized water to remove the loosely adhered protein, rinsed in 1 mL of deionized water and then subjected to 10 minutes of continuous sonication to separate the proteins firmly adhered on the samples. The adhered proteins were quantified on a micro-plate reader using a micro-BCA kit according to the instructions. To observe the resistance of the hydrogel sheets to blood staining, the upper surface of the hydrogel sheets (PVA surface) was soaked with sheep blood and then washed with PBS to observe the residual blood.

Cytocompatibility assay

L929 cells were utilized to investigate the compatibility of the PVA/GA-PAA hydrogel sheet. Firstly, the leachate of a hydrogel sheet immersed in PBS for 24 h was collected. L929 cells were seeded at 1×10^4 cells per well in 24-well plates and cultured using DEME medium with 10% (v/v) of the leachate samples in an incubator at 5% CO_2, 37 °C for a predetermined time (1, 3, or

5 days). A live/dead staining kit was used to detect the cell viability as per the instructions. The stained cells were observed and imaged using a fluorescence microscope (Nikon Ti2, Japan).

Cytotoxicity was analyzed using a cell counting kit (CCK-8). In brief, L929 cells were seeded in 96-well plates with a density of 1×10^3 cells per well and co-cultured using DEME medium with 10% (v/v) of leachate. The medium was removed at the pre-set time, and CCK-8 solution was utilized to detect cell proliferation as per the instruction manual. The yellow solution with CCK-8 was transferred to 96-well plates, and the absorbance value was detected at 450 nm using a microplate reader (Cytation 5, Biotek, USA).

To observe the adhesion of different surfaces to cells, the PVA/GA-PAA hydrogel sheet was cut into a round shape and fixed in a 6-well plate. 2.5×10^4 L929 cells were respectively seeded on both sides of the PVA/GA-PAA hydrogel sheet. After four hours, the PVA/GA-PAA hydrogel sheet was cleaned using deionized water, and the adhered cells were fixed with 2.5% glutaraldehyde. Then, 30%, 50%, 70%, 90%, 95% and 100% ethanol were used for gradient dehydration for 30 minutes. The cell morphology was observed using SEM after drying.

Animal experiment

An incision of 5 mm was created on the intestine of 6 week-old SD rat weighing about 200 g and then sealed using the adhesive PVA/GA-PAA hydrogel sheet. A no-treatment group and a GA-PAA hydrogel sheet group served as the control groups. All operation procedures were conducted under the standard conditions as per the Ethical Committee regulations in China. The rats were sacrificed and photographed for observation of tissue adhesion in the operation position at two weeks post-operation. The repaired wound was prepared into tissue slices, and H&E staining of local wound tissue was used for pathological analysis. The postoperative tissue adhesion scoring was performed as per the international tissue adhesion scoring standards. Scoring grade 0 indicates that no tissue adhesion appears; scoring grade 1 indicates only one thin filmy tissue adhesion; scoring grade 2 means that more than one thin adhesion is present; scoring grade 3 means that there is a thick adhesion with a focal point; scoring grade 4 indicates thick adhesion with plantar attachment or more than one thick adhesion with a focal point; and scoring grade 5 indicates very thick vascularized adhesion or more than one plantar adhesion.

Statistical analysis

Statistical analysis was performed using one-way ANOVA using SPSS 19.0. A p-value < 0.05 was considered statistically significant. $*p < 0.05$, $**p < 0.01$, $***p < 0.001$. NS, not statistically significant. Error bars represent mean $\pm$ SD ($n > 3$).

Results and discussion

FTIR analysis

The PVA/GA-PAA hydrogel sheet was obtained by the initial formation of AA and GA under the action of UV light polymerization and subsequent PVA coating on the surface of one side

(Fig. 1). Fig. 2A shows the FTIR spectra of GA-PAA and PVA/GA-PAA hydrogel sheets. Absorption peaks at 1635 and 1546 cm^{-1} corresponding to the amide I C=O stretching vibration and amide II N–H bending vibration, respectively, can be observed, which can be attributed to gelatin.[23] The absorption peak at 1403 cm^{-1} can be ascribed to the carboxyl group in polyacrylic acid.[24] No evident change is observed after the addition of PVA, except the significantly enhanced absorption peak of the O–H stretching vibration at 3200 cm^{-1}, indicating that PVA was not involved in a chemical reaction, and can form a stable physical barrier on the surface of GA-PAA by hydrogen bonding and polymer entanglement.

XPS analysis

XPS was further applied to validate the chemical structure composition of the PVA/GA-PAA hydrogel sheet. The XPS wide-scan spectra showed the presence of N and C (Fig. 2B). An obvious characteristic peak of N 1s at a binding energy of about 400 eV was observed; however, no significant change in the intensity of N 1s or new bonding energy peaks appeared after the addition of PVA. Through further analysis of the high-resolution N 1s bonding energy spectrum (Fig. 2C and D), the obvious bonding energy peak at 400 eV can be ascribed to NH$_2$ or –N–C=O peaks of PAA or GA.[18] The bonding energy spectra of C 1s showed distinct absorption peaks at 288.6, 284.8, and 286 eV, corresponding to C=O, C–C, and C–OH, respectively, which were mainly from GA and PAA (Fig. 2E and F). No new characteristic peaks appeared in the bonding energy spectrum of C 1s after the addition of PVA.

Morphology observation

The PVA/GA-PAA hydrogel sheet has a transparent appearance, facilitating the direct observation of the wound state when applied for wound closure (Fig. 3A). The microscopic morphology of the hydrogel sheet was further observed using SEM (Fig. 3B). The two sides showed distinct differences in their pore structures, including rough and uniform pores of about 100 μm, which benefit cell growth, in the adhesive surface.[25] Moreover, the rough surface morphology is conducive to the formation of tissue adhesion by the mechanical interlocking effect between the tissue and the adhesion matrix.[26] Nonetheless, the other side shows a dense structure without pores, which can form a stable physical barrier to prevent cell and protein adhesion, and even isolate the internal and external environment of the intestine to avoid infection.[27,28]

Mechanical properties

The good mechanical properties of adhesive hydrogel sheets play a key role in their long-term sustainable adhesion.[29] The results of stress–strain testing showed that the dried hydrogel sheet had a stable elastic modulus in the first strain of 30% (Fig. 4A). The stress of 300 kPa significantly exceeds normal intestinal pressure. In addition, it is found that the PVA/GA-PAA hydrogel sheet had a slight increasing tendency compared to GA-PAA, which can be ascribed to abundant hydrogen bonds derived from the hydroxyl groups of PVA that penetrated into the GA-PAA matrix. Due to the limited content of PVA, the mechanical properties show a small
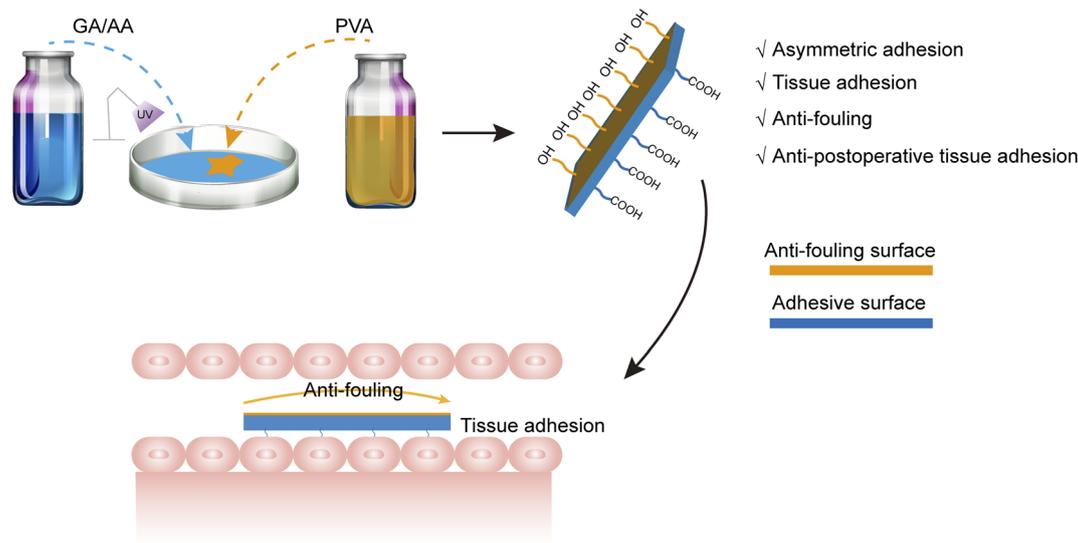
Fig. 1 Schematic illustration of the preparation process of the asymmetrical adhesive hydrogel sheet with anti-fouling performance.

range of improvement, but are superior to those of some adhesive hydrogels reported in the past.[30–32] The ductility of the hydrogel sheet was further observed during stretching. The hydrogel sheet became thin in the middle during stretching and could reach up to seven times elongation, which is beneficial to energy dissipation, increasing the adhesion energy at the interface (Fig. 4B). When the PVA/GA-PAA or GA-PAA hydrogel sheets were immersed in water, their elastic modulus and elongation at break significantly decreased. It can be explained that a large number of water molecules lead to the disruption of hydrogen bonding, increasing

the brittleness of the hydrogel sheets.[33] Despite the decreased elastic modulus, it can meet the intestinal closure requirements.

Adhesion properties

Adhesive biomaterials are capable of achieving rapid sutureless repair of tissue wounds. However, many adhesives show weak adhesion in some tissues, including intestinal tissue, due to the smooth and dense biofilm barrier.[2,34] Herein, the tissue adhesion energy between the PVA/GA-PAA hydrogel sheet and the intestinal surface was examined using a lap-shear test (Fig. 4C).
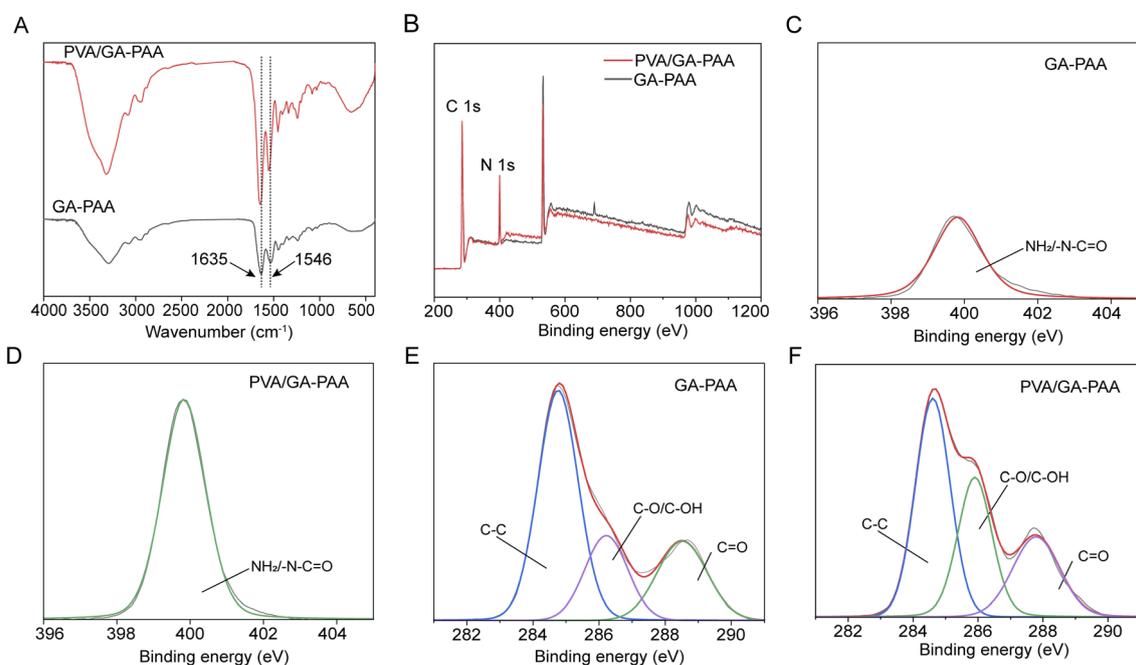

Fig. 2 Structural characterization of the PVA/GA-PAA hydrogel sheet. (A) FTIR spectra of the GA-PAA and PVA/GA-PAA hydrogel sheets. (B) XPS wide-scan spectra. (C and D) Peak-fitting of the XPS spectra in the N 1s regions of the GA-PAA and PVA/GA-PAA hydrogel sheets. (E and F) Peak-fitting of the XPS spectra in the C 1s regions of the GA-PAA and PVA/GA-PAA hydrogel sheets.
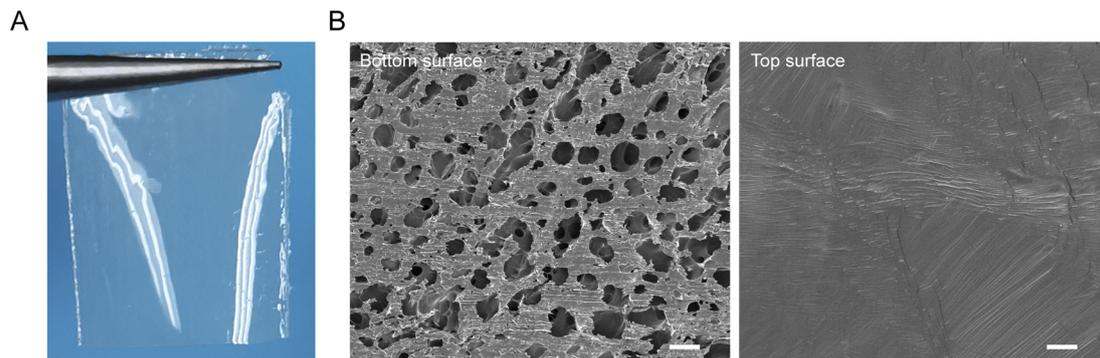
Fig. 3 (A) Photograph of the prepared PVA/GA-PAA hydrogel sheet. (B) SEM images of the surfaces of the two sides of the PVA/GA-PAA hydrogel sheet. Scale bars: 200 μm.

The results showed that the two sides of the GA-PAA hydrogel sheet showed tissue adhesion, reaching a maximum adhesion strength of 12.6 kPa (Fig. 4D). Only one side of PVA/GA-PAA is adhesive, and it reached a maximum adhesion strength of 25.8 kPa. The remarkable increase can be ascribed to the better energy dissipation due to PVA with abundant –OH providing more reversible hydrogen bonds inside the PVA/GA-PAA hydrogel sheet. In addition, it can be inferred that the dried PVA/GA-PAA hydrogel sheets can better absorb the free water on the tissue surface to enhance the interfacial adhesion energy due to the additional hydrophilicity of PVA. The stress–strain curve of tissue adhesion shows that the loading force does not disappear immediately after de-adhesion, demonstrating that the hydrogel sheet shows good flexibility, unlike most brittle hydrogels. At the same time, the PVA coating on the surface of the PVA/GA-PAA hydrogel sheet shields the redundant adhesion, reducing the risk of postoperative adhesion complications.

Protein adsorption

Postoperative tissue adhesion can be caused by an excessive fibrotic reaction resulting from aggravated inflammation in addition to immediate abnormal adhesion of the material.[22] As
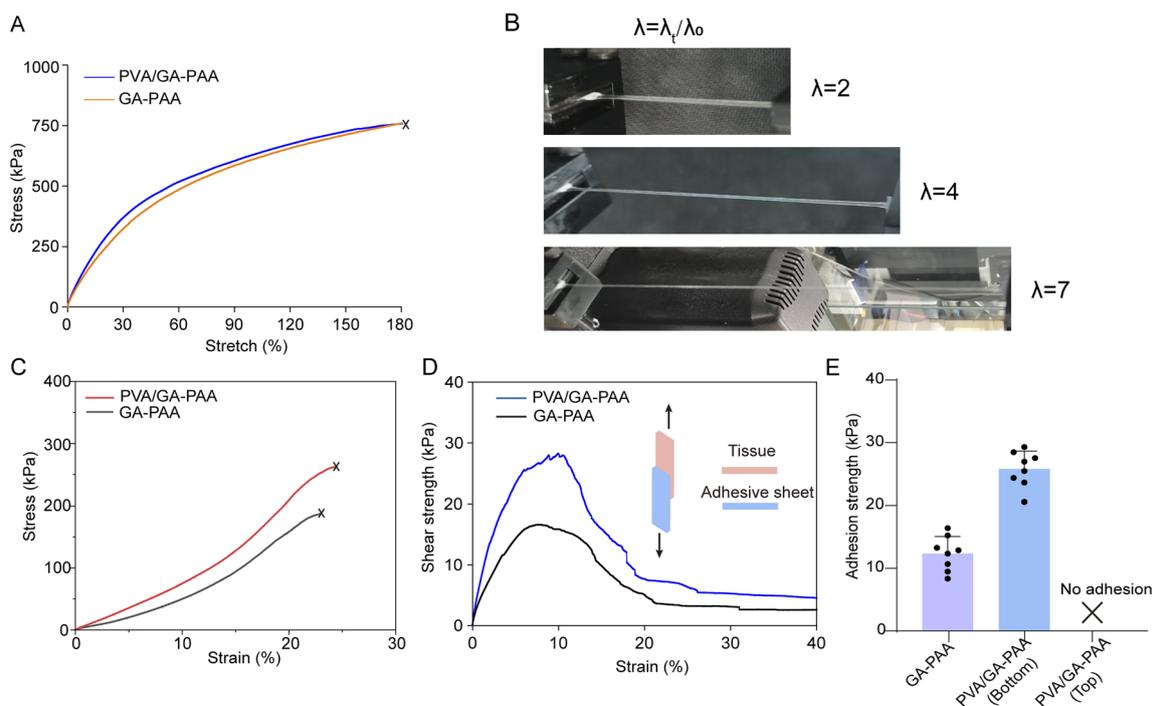

Fig. 4 Characterization of the mechanical properties and adhesive performance. (A) Stress–strain curves of GA-PAA and PVA/GA-PAA hydrogel sheets. (B) Photographs of PVA/GA-PAA hydrogel sheets stretched to more than seven times their original length. (C) Stress–strain curves of GA-PAA and PVA/GA-PAA hydrogel sheets in the water-equilibrated state. (D) Shear strength *versus* strain for porcine intestine adhered using the GA-PAA and PVA/GA-PAA hydrogel sheets. (E) Maximal adhesion strength of the GA-PAA and PVA/GA-PAA hydrogel sheets (top and bottom surfaces).

Paper

RSC Advances

a matter of fact, the fast recognition of a foreign body by the organism generating a systemic immune response will exacerbate inflammation in the wound, triggering an excessive fibrotic reaction to form a scar. Therefore, anti-protein adhesion ability plays a vital role in resisting biological contamination, evading immune system attack, and reducing the risk of postoperative adhesion.[35] According to the protein adsorption results (Fig. 5A and B), pure PVA or a PVA coating on the surface of the PVA/GA-PAA hydrogel sheet showed adsorption ratios lower than 0.5 μg cm^{-2} for the representative proteins BSA and fibrin; however, the other side of the PVA/GA-PAA hydrogel sheet shows a capacity for asymmetric biological adhesion with a high adhesion rates for both proteins. As reported, adhesion rates of 1 μg cm^{-2} indicate postoperative anti-adhesion potential.[18]

Cell adhesion experiments further confirmed that the top surface can effectively prevent cell adhesion, but the bottom does not affect cell adhesion. It can be inferred that the blood mainly includes protein and blood cells, and cell adhesion is ascribed to the protein integrin. Therefore, the PVA/GA-PAA hydrogel sheet showed anti-adhesive capacity toward cells. Inspired by this, the PVA/GA-PAA hydrogel sheet can be beneficial for *in vivo* anti-adhesion.

Biocompatibility

To assess the biocompatibility of the PVA/GA-PAA hydrogel sheets, CCK-8 and live–dead staining analysis were performed. The results of co-culturing with the samples revealed that the L929 cells can rapidly proliferate on day 1, 3, and 5 without significant density differences between the PVA/GA-PAA, GA-PAA, and control groups, indicating that PVA/GA-PAA does not affect the growth of L929 (Fig. 5C). The live–dead staining results validated that L929 cells showed the normal state with a shuttle-shaped morphology and similar proliferation rates between all the groups for 5 days (Fig. 5D).

Evaluation of postoperative adhesion prevention *in vivo*

All animal procedures were performed in accordance with the Guidelines for Care and Use of Laboratory Animals of Guangzhou Huateng Biomedical Technology Co., Ltd., and approved by the Animal Ethics Committee of Guangzhou Huateng Biomedical Technology Co., Ltd. Inspired by the good biocompatibility and stable amphipathic properties *in vitro*, a rat intestinal injury model was constructed to assess the capacity of the PVA/GA-PAA hydrogel sheet for wound sealing without postoperative tissue adhesion *in vivo* (Fig. 6A). A 5 mm incision in the rat intestine was treated with GA-PAA or PVA/GA-PAA. PVA/GA-PAA showed
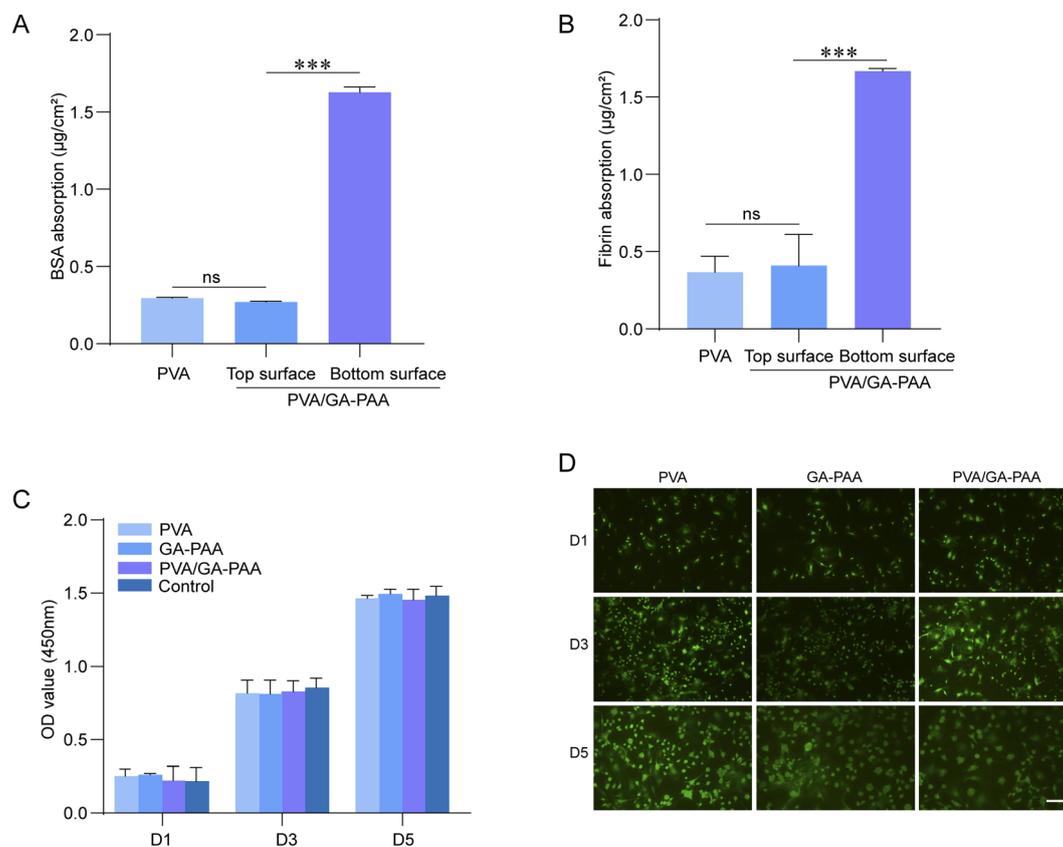

Fig. 5 Anti-fouling performance and biocompatibility of the hydrogel sheet. (A and B) BCA measurements of BSA and fibrin absorption on the surfaces of the two sides of the PVA/GA-PAA hydrogel sheets and PVA alone. (C) L929 cell proliferation on PVA, GA-PAA and PVA/GA-PAA hydrogel sheets after culturing for 1, 3 and 5 days. The blank group was the control group. (D) L929 cell viability after culturing in PVA, GA-PAA and PVA/GA-PAA hydrogel sheets for two days as determined using live/dead staining: live (green), dead (red). Scale bars: 200 μm.
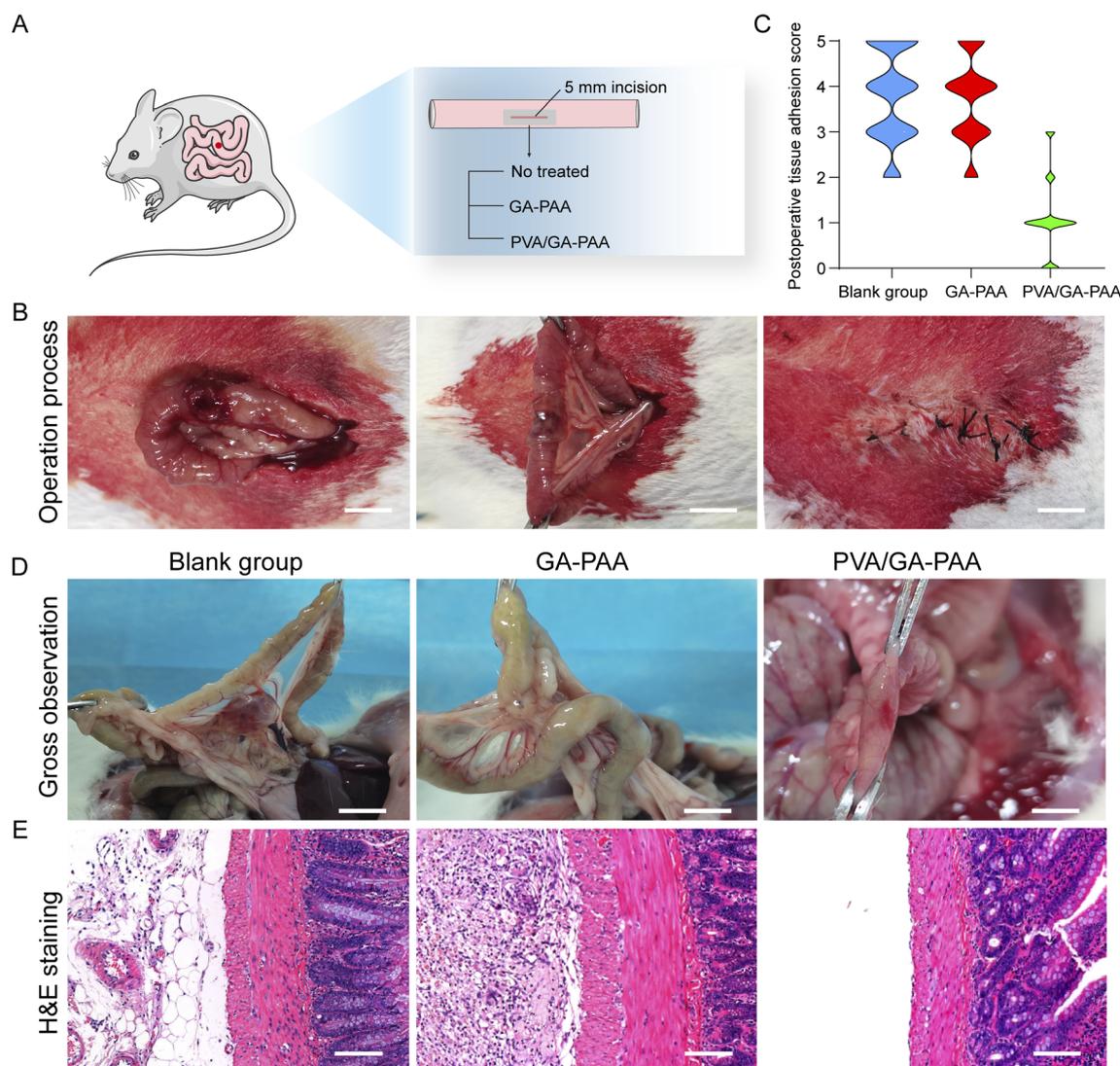
Fig. 6 (A) Schematic illustration of intestinal repair in the rat model. (B) Operation photographs of injured intestine sealed by the adhesive PVA/GA–PAA hydrogel sheet. Scale bars: 10 mm. (C) Postoperative tissue adhesion scores 14 days after surgery in the blank, GA–PAA and PVA/GA–PAA hydrogel sheet groups. (D) Gross observation of the repaired intestine 14 days after surgery. Scale bars: 10 mm. (E) Pathological analysis using H&E in the blank, GA–PAA and PVA/GA–PAA hydrogel sheet groups 14 days after surgery. Scale bars: 100 μm.

significant hemostasis of the wound during surgery (Fig. 6B). At two weeks post-operation, the rats were sacrificed to observe the injured intestine. The control and GA-PAA groups showed a serious tissue adhesion state with maximum adhesion scores according to the international standard assessment, while the PVA/GA-PAA group had almost no adhesion with the lowest scores (Fig. 6C and D). Ectopic adhesion was also observed in addition to wound adhesion in the control and blank groups. It can be speculated that the blank group experienced infection in the abdominal cavity due to the indulgent leaks, and the GA-PAA group was prone to acute adhesion due to surface physical adhesion. No significant inflammatory or tissue adhesion was observed in the PVA/GA-PAA hydrogel sheet group. According to the pathological analysis of histological sections, the epithelial tissue in the control group was not repaired, with obvious plasma membrane adhesion. The GA-PAA group showed significant inflammatory cells, fibroblast aggregation, and adhesion tissue, while the experimental group showed obvious boundaries between the plasma membrane and the surrounding normal intestinal tissues without tissue adhesion (Fig. 6E).

Conclusions

In summary, a PVA/GA-PAA hydrogel sheet with asymmetric tissue adhesion was successfully prepared. Tough adhesion under wet conditions, stable mechanical properties, favorable biocompatibility, and remarkable anti-fouling capacity allow the PVA/GA-PAA hydrogel sheet to achieve fast wound sealing of injuries without postoperative tissue adhesion. The perfect combined strategy of opposite performances provides the

adhesives with promising insight into clinical application in the future.

Conflicts of interest

There are no conflicts to declare.

Acknowledgements

Notes and references

1 N. J. Turner, S. A. Johnson, L. J. R. Foster and S. F. Badylak, *J. Biomed. Mater. Res., Part B*, 2018, **106**, 1698–1711.

2 J. Wu, H. Yuk, T. L. Sarrafian, C. F. Guo, L. G. Griffiths, C. S. Nabzdyk and X. Zhao, *Sci. Transl. Med.*, 2022, **14**, eabh2857.

3 A. Gonzalez-Sagredo, M. Gil, M. D'Oria, K. Spanos, A. Salinas, S. Matus, T. Carnaval, S. Llagostera, S. Lepidi, A. Giannoukas, S. Bellmunt, R. Garcia-Vidal, S. Videla, R. Vila and E. Iborra, *Medicine*, 2022, **101**, e31800.

4 J. Li, A. D. Celiz, J. Yang, Q. Yang, I. Wamala, W. Whyte, B. R. Seo, N. V. Vasilyev, J. J. Vlassak, Z. Suo and D. J. Mooney, *Science*, 2017, **357**, 378–381.

5 J. H. Kim, H. Kim, Y. Choi, D. S. Lee, J. Kim and G. R. Yi, *ACS Appl. Mater. Interfaces*, 2017, **9**, 31469–31477.

6 M. A. Gonzalez, J. R. Simon, A. Ghoorchian, Z. Scholl, S. Lin, M. Rubinstein, P. Marszalek, A. Chilkoti, G. P. López and X. Zhao, *Adv. Mater.*, 2017, **29**, 1604743.

7 V. Bhagat and M. L. Becker, *Biomacromolecules*, 2017, **18**, 3009–3039.

8 A. Assmann, A. Vegh, M. Ghasemi-Rad, S. Bagherifard, G. Cheng, E. S. Sani, G. U. Ruiz-Esparza and N. Annabi, *Biomaterials*, 2017, **140**, 115–127.

9 H. Yuk, C. E. Varela, C. S. Nabzdyk, X. Mao, R. F. Padera, E. T. Roche and X. Zhao, *Nature*, 2019, **575**, 169–174.

10 L. Gao, M. Xu, W. Zhao, T. Zou, F. Wang, J. Da, Y. Wang and L. Wang, *Bioact. Mater.*, 2022, **18**, 128–137.

11 M. Li, W. Li, Q. Guan, X. Dai, J. Lv, Z. Xia, W. J. Ong, E. Saiz and X. Hou, *ACS Nano*, 2021, **15**, 19194–19201.

12 E. Zhang, B. Song, Y. Shi, H. Zhu, X. Han, H. Du, C. Yang and Z. Cao, *Proc. Natl. Acad. Sci. U. S. A.*, 2020, **117**, 32046–32055.

13 J. Yu, K. Wang, C. Fan, X. Zhao, J. Gao, W. Jing, X. Zhang, J. Li, Y. Li, J. Yang and W. Liu, *Adv. Mater.*, 2021, **33**, e2008395.

14 E. Zhang, J. Yang, K. Wang, B. Song, H. Zhu, X. Han, Y. Shi, C. Yang, Z. Zeng and Z. Cao, *Adv. Funct. Mater.*, 2021, **31**, 2009431.

15 L. M. Stapleton, A. N. Steele, H. Wang, H. L. Hernandez, A. C. Yu, M. J. Paulsen, A. A. A. Smith, G. A. Roth and Y. J. Woo, *Nat. Biomed. Eng.*, 2019, **3**, 611–620.

16 C. Y. Cui, T. L. Wu, X. Y. Chen, Y. Liu, Y. Li, Z. Y. Xu, C. C. Fan and W. G. Liu, *Adv. Funct. Mater.*, 2020, **30**, 2005689.

17 C. J. Huang, Y. Li and S. Jiang, *Anal. Chem.*, 2012, **84**, 3440–3445.

18 X. Chen, Z. Lin, Y. Feng, H. Tan, X. Xu, J. Luo and J. Li, *Small*, 2019, **15**, e1903784.

19 W. W. Liang, W. Y. He, R. K. Huang, Y. C. Tang, S. M. Li, B. N. Zheng, Y. Y. Lin, Y. H. Lu, H. Wang and D. C. Wu, *Adv. Mater.*, 2022, **34**, 2108992.

20 S. H. Bae, S. R. Son, S. Kumar Sakar, T. H. Nguyen, S. W. Kim, Y. K. Min and B. T. Lee, *J. Biomed. Mater. Res., Part B*, 2014, **102**, 840–849.

21 X. Cai, S. Hu, B. Yu, Y. Cai, J. Yang, F. Li, Y. Zheng and X. Shi, *Carbohydr. Polym.*, 2018, **201**, 201–210.

22 H. Park, S. Baek, H. Kang and D. Lee, *Materials*, 2020, **13**, 3056.

23 F. Zhang, C. He, L. Cao, W. Feng, H. Wang, X. Mo and J. Wang, *Int. J. Biol. Macromol.*, 2011, **48**, 474–481.

24 Y. Cheng, Y. Hu, M. Xu, M. Qin, W. Lan, D. Huang, Y. Wei and W. Chen, *J. Biomater. Sci., Polym. Ed.*, 2020, **31**, 1836–1851.

25 W. Yang, H. Xu, Y. Lan, Q. Zhu, Y. Liu, S. Huang, S. Shi, A. Hancharou, B. Tang and R. Guo, *Int. J. Biol. Macromol.*, 2019, **130**, 58–67.

26 H. Yuk, T. Zhang, S. Lin, G. A. Parada and X. Zhao, *Nat. Mater.*, 2016, **15**, 190–196.

27 Z. Li, A. Milionis, Y. Zheng, M. Yee, L. Codispoti, F. Tan, D. Poulikakos and C. H. Yap, *Nat. Commun.*, 2019, **10**, 5562.

28 Z. Luo, L. Jiang, C. F. Xu, D. Kai, X. S. Fan, M. L. You, C. M. Hui, C. S. Wu, Y. L. Wu and Z. B. Li, *Chem. Eng. J.*, 2021, **421**, 127725.

29 T. Kurokawa, H. Furukawa, W. Wang, Y. Tanaka and J. P. Gong, *Acta Biomater.*, 2010, **6**, 1353–1359.

30 N. Han, Z. Xu, C. Cui, Y. Li, D. Zhang, M. Xiao, C. Fan, T. Wu, J. Yang and W. Liu, *Biomater. Sci.*, 2020, **8**, 3164–3172.

31 B. R. Freedman, O. Uzun, N. M. M. Luna, A. Rock, C. Clifford, E. Stoler, G. Ostlund-Sholars, C. Johnson and D. J. Mooney, *Adv. Mater.*, 2021, **33**, e2008553.

32 X. He, N. Wen, W. Zhang, S. He, S. Yang, X. Li, C. Chen and F. Zuo, *RSC Adv.*, 2023, **13**, 7561–7568.

33 Y. W. Huang, S. Y. Qian, J. Zhou, W. J. Chen, T. Liu, S. Yang, S. J. Long and X. F. Li, *Adv. Funct. Mater.*, 2023, **33**, 2213549.

34 L. Wang, F. Liu, X. Zhai, W. Dong, W. Wei and Z. Hu, *Int. J. Biol. Macromol.*, 2023, **241**, 124622.

35 B. D. Ratner and S. J. Bryant, *Annu. Rev. Biomed. Eng.*, 2004, **6**, 41–75.